Discovery of the Quiescent Body that Functions as a Biological Timer for Growth Resumption of Non-growing Bacterial Cells

Jiayu Yu[1†], Yang Liu[1†] & Zengyi Chang[1,2,*]

[1]The State Key Laboratory of Protein and Plant Gene Research, School of Life Sciences, Peking University, Beijing 100871, P.R. China
[2]Center for Protein Science, Peking University, Beijing 100871, P.R. China
[†]J.Y. and Y.L. contributed equally to this work
[*]Correspondence: changzy@pku.edu.cn (Z.C.)

Abstract

Bacterial cells in natural environment often exist in a non-growing state. They recover after a short or long lag time when encountering a growth-supportive condition. Such dormant bacteria are known for their high tolerance towards adverse conditions such as the presence of antibiotics and are thus viewed as a great challenge for the treatment of infectious diseases. Nevertheless, it remains poorly understood on how bacterial cells enter such an inert state and why a heterogeneous lag time is taken before they could recover. In this study, we accidentally discovered a subcellular structure that we term quiescent body, which is formed in the non-growing/non-dividing stationary-phase *E. coli* cells and selectively sequesters many proteins essential for cell growth, division and metabolism. This finding was made when we tried to trace the status of FtsZ, an essential protein for bacterial cytokinesis, via *in vivo* protein photo-crosslinking and live-cell fluorescence microscopic imaging. We further demonstrated the following. 1. Formation of quiescent bodies can be induced by indole and relies on the occurrence of cellular respiration. 2. When the non-growing cells are placed in fresh culture medium, the quiescent bodies will initiate their dissolution in cells that have started to re-grow, releasing the sequestered proteins for functional resumption, but remain unaltered in cells that have not yet started their re-growth. 3. Both the formation and dissolution of quiescent bodies occur in a highly heterogeneous manner among individual cells, and that the degree of their formation is highly correlated with the duration of the lag time taken for bacterial cells to recover. These findings strongly implicate that the quiescent bodies function as a biological timer for growth resumption of the non-growing cells. The maintenance of quiescent body possibly represents a distinguishing feature and is thus helpful for an unequivocal identification of such hitherto elusive dormant (persister) bacterial cells. Our findings shed light not only on how and why a lag time is taken, but also on inventing new ways to eradicate the multidrug-tolerant pathogens, for

example, by blocking the formation or promoting the dissolution of quiescent bodies in them.

Introduction

Bacterial cells in the natural environment are considered to mainly exist in a non-growing/non-dividing dormant state. One remarkable feature of such inert cells is their capacity to survive under adverse conditions, such as the high temperature (i.e., boiling) or the presence of any antibiotic[1–3]. Meanwhile, it has long been recognized that the non-growing/non-dividing bacterial cells commonly take a lag time, heterogeneous among the individual cells, before resuming growth when encounter a growth-supportive condition[4–6]. The lag time is associated with the invasiveness of pathogens and antibiotic tolerance[7–10]. Recently, it has been suggested that an extended lag time correlated to an increased tolerance towards antibiotics and this 'tolerance by lag' may further facilitate the subsequent evolution of antibiotic resistance[11,12]. Nevertheless, it remains poorly understood on how and why a heterogeneous lag time exists before they recover, mainly due to the low density or inert metabolic activities for these cells.

Here, we discovered a reversible subcellular structure and termed it as the quiescent body, which sequesters selected essential proteins and is formed in the non-growing/non-dividing late stationary-phase *E. coli* cells but is dissolved when the cells resume growth in fresh medium. We further demonstrated that the degree of quiescent body formation is strongly correlated with the duration of lag time for bacterial cells to recover, and it apparently functions as a biological timer for the growth resumption of such non-growing bacterial cells.

The finding of quiescent body was made accidentally by us while performing the unnatural amino acid-mediated protein photo-crosslinking analysis to decipher the assembling pattern of the cell division protein FtsZ, a homolog of the eukaryotic tubulin protein[13,14] and whose monomers are known to self-associate into fibrous protofilaments by using two longitudinal interfaces under *in vitro* conditions[15,16], in living *E. coli* cells. Such protofilaments are believed to further assemble, via an undefined manner, into the Z-ring structure in the middle of each cell before generating constriction during cytokinesis[17,18]. While commonly performed our *in vivo* protein photo-crosslinking analysis on FtsZ in the actively dividing log-phase cells, we once did a similar analysis on the non-dividing late stationary-phase cells, assuming that the FtsZ protein would exist as monomers in them. We found, strikingly, that a large portion of the FtsZ monomers in the late stationary-phase cells, though indeed no longer self-assemble into protofilaments, exist in the insoluble pellet fraction of the cell lysates. We subsequently demonstrated by live-cell imaging analysis that the FtsZ proteins in late stationary-phase cells largely exist in a type of cell-pole granules which also contain many other functionally important proteins. We then revealed that when such non-dividing cells were inoculated in fresh culture

83 medium, the cell-pole granules, which we termed as quiescent bodies, were
84 effectively dissolved in the re-growing cells, with the sequestered FtsZ protein being
85 relocated into the Z-ring structure. By contrast, those cells that maintained their
86 quiescent bodies intact did not initiate their re-growth, thus displaying a significantly
87 longer lag time. Notably, we found that both the formation (upon entering the
88 stationary phase) and dissolution (during the recovery) occur in a highly
89 heterogeneous manner among the individual cells.
90 The quiescent body that we unveiled here apparently acts as a biomarker for an
91 efficient and unequivocal identification of the hitherto elusive dormant or persister
92 bacterial cells. More importantly, they conceivably function as a biological timer that
93 defines the duration of lag time for the non-growing bacterial cells to resume growth.
94
95 ## Results
96
97 **The FtsZ protein interacts with multiple other proteins and exists in the**
98 **insoluble pellet fraction of non-dividing late stationary-phase *E. coli* cells.**
99 The determined crystal structure of the FtsZ protofilaments reveals a head-to-tail
100 longitudinal assembling pattern of the FtsZ monomers[19,20]. In light of this structural
101 information, we initially tried to confirm whether or not such observed assembling
102 pattern indeed exists in living *E. coli* cells, and meanwhile to identify other interaction
103 surfaces that would allow such protofilaments to further assemble into the
104 higher-order Z-ring. To this end, we performed a systematic *in vivo* protein
105 photo-crosslinking analysis on FtsZ, as mediated by the genetically incorporated
106 unnatural amino acid p-benzoyl-L-phenylalanine (pBpa)[21,22], which has been
107 routinely and effectively used in our laboratory[23–25]. Among the pBpa variants we
108 prepared, FtsZ-K140pBpa was one in which the residue K140, that is reported to
109 locate at the longitudinal interface[19,26], was replaced by pBpa. We first confirmed that
110 FtsZ-K140pBpa is able to substitute the wild-type FtsZ protein in supporting cell
111 division (**Fig. S1A**), ruling out any occurrence of major structural disruptions.
112 To unequivocally demonstrate whether or not the residue K140 indeed resides in
113 the longitudinal assembling surface of FtsZ in living cells, besides heterologously
114 expressing FtsZ-K140pBpa, we also modified the genomic *ftsZ* gene to produce an
115 Avi-tagged FtsZ form, designated as FtsZ-Avi, which can thus be detected by using
116 the streptavidin-alkaline phosphatase conjugate (abbreviated as streptavidin-AP
117 conjugate) that specifically probes the Avi tag. As shown by the blotting results
118 displayed in **Fig. 1A,** such FtsZ dimers were clearly detected in the actively dividing
119 log-phase cells, either as one band probed with streptavidin-AP conjugate (lane 2, red
120 arrow; formed between FtsZ-K140pBpa and FtsZ-Avi), or as a doublet band probed
121 with anti-FtsZ antibodies (lane 6, red and black arrows; the bottom band formed
122 between two FtsZ-K140pBpa monomers). These results confirm that the residue
123 K140 indeed locates at the self-assembling interface of FtsZ to form protofilaments in
124 living cells.

125 Out of curiosity, we also performed the above photo-crosslinking experiments
126 with the non-dividing/non-growing late stationary-phase cells, assuming that the
127 head-to-tail protofilaments would no longer exist. The results, also displayed in **Fig.**
128 **1A**, clearly show that the photo-crosslinked dimer between FtsZ-K140pBpa and
129 FtsZ-Avi became no longer detectable when probed with the streptavidin-AP
130 conjugate (lane 4), indicating that the FtsZ protofilaments are indeed no longer
131 maintained in such cells. However, when probed with antibodies against FtsZ,
132 multiple photo-crosslinked non-dimer products of FtsZ-K140pBpa were detected (**Fig.**
133 **1A,** lane 8). This indicates that the FtsZ monomer, although no longer self-associates,
134 now interacts with multiple other proteins via the original longitudinal interface.
135 Apparently, these interactions may prevent the FtsZ monomers to self-associate into
136 the protofilaments in the non-dividing cells.
137 We next tried to identify the proteins that interact with FtsZ in the late
138 stationary-phase cells. For this purpose, we initially attempted to purify the
139 photo-crosslinked products of FtsZ-K140pBpa (e.g., through immunoprecipitation)
140 before subjecting them to mass spectrometry analysis. During the purification,
141 however, we strikingly found that not only almost all the photo-crosslinked products
142 of FtsZ-K140pBpa but also a large portion of the two types of free FtsZ monomers
143 were detected in insoluble pellet fraction of the cell lysates (**Fig. 1B**, lane 8), while
144 the photo-crosslinked FtsZ dimers and the free FtsZ monomers were both detected in
145 the soluble supernatant (**Fig. 1B**, lane 3), hardly any in the insoluble pellet (**Fig. 1B**,
146 lane 4) fraction of the log-phase cells.
147 To rule out the possibility that the detection of FtsZ monomers in the pellet
148 fraction was an artifact due to the introduction of the pBpa residue or the Avi tag in
149 the FtsZ protein and/or the UV irradiation, we then analyzed the distribution of the
150 endogenous FtsZ protein in the supernatant and pellet fractions of the late
151 stationary-phase wild-type *E. coli* cells. Our immunoblotting results, displayed in **Fig.**
152 **1C**, clearly demonstrate that the endogenous FtsZ protein is similarly detected largely
153 in the pellet fraction (top panel, lane 6) of late stationary-phase cells, with little in the
154 pellet fraction (lane 3) of the log-phase cells. For comparison, we found that EF-Tu
155 (as one of the most abundant proteins) and GroEL (as a molecular chaperone protein
156 that usually interacts with unfolded client proteins) were both detected largely in the
157 supernatant (lane 5), hardly in the pellet (lane 6) of late stationary-phase cells (**Fig.**
158 **1C**, middle and bottom panels, respectively). Taken together, these results strongly
159 suggest that the FtsZ proteins apparently exist as insoluble forms in late
160 stationary-phase *E. coli* cells.

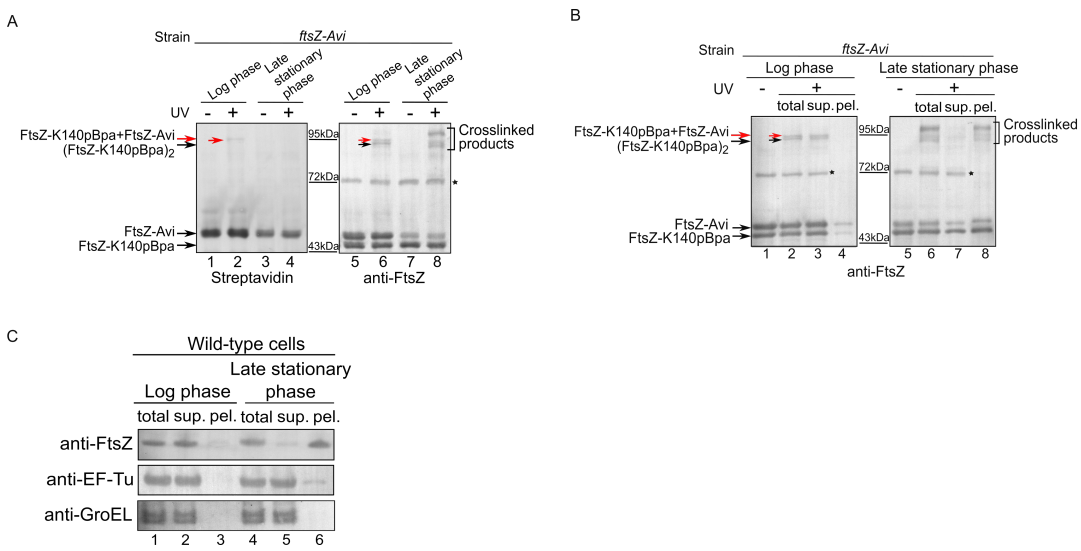

Figure 1. The FtsZ protein is detected in the insoluble pellet fraction of non-dividing late stationary-phase *E. coli* cells.

(A) Blotting results for detecting photo-crosslinked products of the FtsZ-K140pBpa variant in log-phase and late stationary-phase cells of the *ftsZ-Avi* strain, probed with the streptavidin-AP conjugate (Streptavidin) or antibodies against FtsZ protein (Anti-FtsZ). Indicated on the left are positions of the two indicated monomers and the two photo-crosslinked dimers, indicated in the middle are positions of the molecular weight markers, indicated on the right are positions of photo-crosslinked products formed between FtsZ-140pBpa and other non-FtsZ proteins. The asterisk indicates a non-specific protein band generated when probed with the anti-FtsZ antibodies.

(B) Immunoblotting results for detecting the photo-crosslinked products and free monomers in the supernatant (sup.) and pellet (pel.) fractions of the log-phase or late stationary-phase *ftsZ-Avi* cells expressing the FtsZ-K140pBpa variant, probed with antibodies against FtsZ. The asterisk indicates the same non-specific protein band as described in (**A**). Positions of the bands are similarly indicated as in (**A**).

(C) Immunoblotting results for detecting the endogenous FtsZ, EF-Tu or GroEL in the total cell lysate (total), the supernatant (sup.) and the pellet (pel.) fractions of log-phase or late stationary-phase wild-type *E. coli* cells, probed with the indicated antibodies.

It should be pointed out that in late stationary-phase cells a significant amount of the monomers for either FtsZ-K140pBpa or FtsZ-Avi were detected in the supernatant fraction of the transformed *E. coli* cells (panel **B**, lane 7), while the endogenous FtsZ in the wild-type cells are largely detected in the pellet fraction (panel **C**, lane 5). This is most likely due to the fact that the total amount of the FtsZ proteins, as represented by both FtsZ-K140pBpa and FtsZ-Avi, in the transformed cells is significantly higher than that of the endogenous FtsZ in the wild-type cells.

The FtsZ protein exists in cell-pole granules in the late stationary-phase *E. coli* cell.

We next attempted to gain further insight into the status of FtsZ protein in late stationary-phase *E. coli* cells by performing live-cell fluorescence microscopic imaging analysis. For this purpose, we labeled the FtsZ protein with the green fluorescent protein mNeonGreen by generating the FtsZ-mNeonGreen fusion protein and heterologously expressed it in wild-type *E. coli* cells, similar to what was reported before by others[27]. We confirmed, as shown in **Fig. 2A** (top part) that this FtsZ-mNeonGreen fusion protein is effectively incorporated into and thus labels the Z-ring structure in the middle of actively dividing log-phase cells.

198 We then subjected the late stationary-phase cells to similar live-cell imaging
199 analysis, and revealed, of great interest, that the FtsZ-mNeonGreen proteins were
200 largely detected in two granules that locate at the two cell poles (**Fig. 2A**, bottom part).
201 For comparison, the similarly expressed unfused mNeonGreen protein was found to
202 be evenly distributed in the cytoplasm of either log-phase (top panel) or late
203 stationary-phase (bottom panel) cells (**Fig. S1C**). Subsequent three-dimensional
204 fluorescence imaging analysis (as displayed in **Movie S1)** showed that such cell-pole
205 granules take a shape of ellipsoid (**Fig. 2A**, bottom row, enlarged images) whose
206 ellipticity was calculated to be 0.35 ± 0.065 ($n > 200$). It is pertinent to note that such
207 an ellipsoid shape is dramatically different from the spherical or rod shape as
208 commonly taken by inclusion bodies, being a structure commonly formed by a
209 particular protein that is over-expressed in bacterial cells [28]. Consistent with what we
210 observed above (**Figs. 1B** and **1C**), a majority of either the endogenous FtsZ or the
211 heterologously expressed FtsZ-mNeonGreen was detected in the pellet fraction of the
212 late stationary-phase cells (**Fig. 2B**, lane 6), but in the supernatant fraction of the
213 log-phase cells (**Fig. 2B**, lane 2). Collectively, these results demonstrate that the FtsZ
214 protein in non-dividing late stationary-phase cells no longer exists as the Z-ring
215 structure but as a form of cell-pole granules.
216 We then tried to further clarify the subcellular localization of such cell-pole
217 granules. For this purposes, we first constructed an *E. coli* strain whose *rhaBAD* gene
218 in the rhamnose operon was replaced by a gene encoding the FtsZ-mNeonGreen
219 protein, such that the expression of the latter is directed by the rhamnose-inducible
220 promoter, as illustrated in **Fig. S1D** (top panel). We verified that the
221 FtsZ-mNeonGreen protein is produced only in the presence of rhamnose (**Fig. S1D**,
222 bottom left panel) and the production of FtsZ-mNeonGreen hardly affected the
223 normal growth of the cells (**Fig. S1D**, bottom right panel). Similarly, the Z-ring in
224 log-phase cells and the cell-pole granules in late stationary-phase cells were observed
225 for the *ftsZ-mNeonGreen* strain when cultured in the presence of rhamnose (**Fig.
226 S1E**).
227 We then separately labeled the outer membrane with OmpA (an outer membrane
228 protein)-fused red fluorescent protein mCherry[29] (**Fig. 2C**, top panel), the inner
229 membrane with the inner membrane anchoring peptide (derived from the nlpA
230 protein)-fused mCherry[30] (**Fig. 2C**, middle panel) and the cytosol with the unfused
231 mCherry (**Fig. 2C**, bottom panel) in the *ftsZ-mNeonGreen* strain. The live-cell
232 imaging data displayed in **Fig. 2C** clearly show that the cell-pole granules occupy a
233 cytosolic location which is hardly accessible to the cytosolic mCherry proteins
234 (bottom panel), suggesting that the structure of the granules are rather compact.
235 Collectively, these imaging data unequivocally demonstrate that, in late
236 stationary-phase cells, the FtsZ protein largely exists in the compact cell-pole
237 granules with a shape significantly different from that of inclusion bodies.

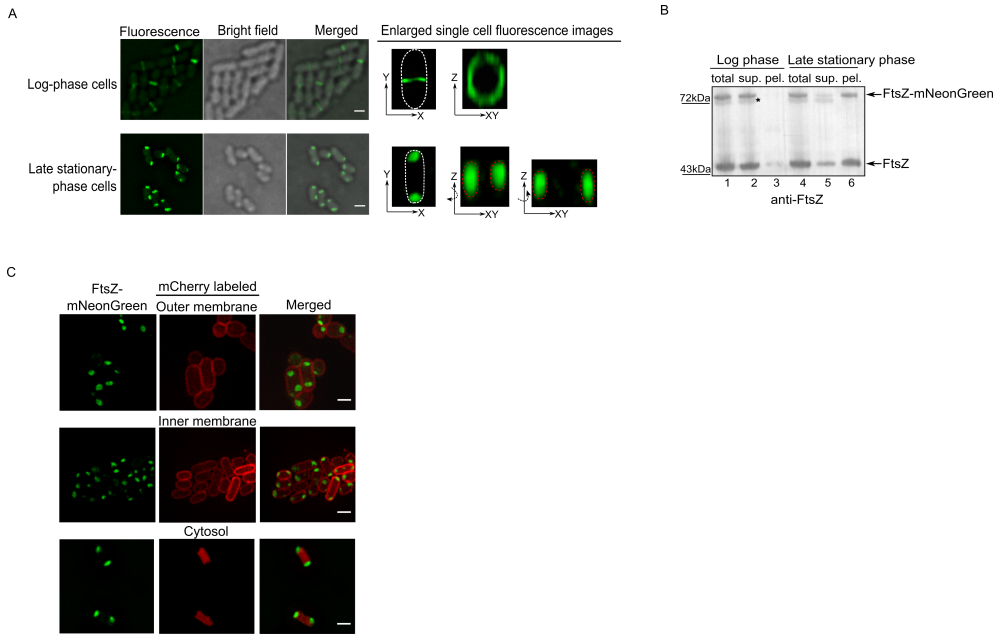

Figure 2. The heterologously expressed FtsZ-mNeonGreen protein exists in a form of cell-pole granules in late stationary-phase *E. coli* cells.

(A) Fluorescence and bright field microscopic images of the log-phase (cultured to 6 h; top panel) and late stationary-phase (cultured to 24 h; bottom panel) *E. coli* cells in which the FtsZ-mNeonGreen protein, besides the endogenous FtsZ protein, was heterologously expressed from a plasmid. Enlarged single cell fluorescent images are also displayed for a better view of the Z-ring structure (in the log-phase cells) and the cell-pole granules (in late stationary-phase cells). Scale bars, 1 μm.

(B) Immunoblotting results for detecting both the endogenous FtsZ and the heterologously expressed FtsZ-mNeonGreen in the total cell lysate (total), supernatant (sup.) and pellet (pel.) fractions of log-phase or late stationary-phase cells, probed with antibodies against FtsZ. Positions of FtsZ and FtsZ-mNeonGreen are indicated on the right and of the molecular weight markers on the left. The asterisk indicates the non-specific protein band.

(C) Fluorescence microscopic images of late stationary-phase *ftsZ-mNeonGreen* cells whose outer membrane (top), inner membrane (middle) or cytosol (bottom) was separately labeled via the fused mCherry (for the two membranes) or unfused mCherry (for the cytosol). Scale bars, 1 μm.

The cell-pole granule or quiescent body selectively sequesters proteins that are vital to cell growth and division.

After searching the literatures, we noticed a report that described the isolation (via sucrose gradient centrifugation) of a multi-protein aggregates which are only formed in stationary-phase *E. coli* cells [31]. However, without a further analysis on the status of the proteins, the authors assumed that such aggregates are made of misfolded proteins and destined for degradation. As a matter of fact, it remains a great challenge to directly demonstrate whether a protein in such insoluble structures is folded or not even under *in vitro* conditions, let alone in living cells. Despite of this, we made an effort to find out whether the FtsZ proteins residing in the cell-pole granules are folded, noting that the FtsZ protein was reported not to form inclusion bodies when over-expressed in bacterial cells[32].

270 To this end, we again exploited the *in vivo* protein photo-crosslinking analysis
271 mediated by the unnatural amino acid pBpa, assuming that the pBpa variants of FtsZ
272 protein would form photo-crosslinked products with other proteins in a
273 surface-specific manner if it is folded[33]. Specifically, we performed the *in vivo* protein
274 photo-crosslinking in late stationary-phase cells for a number of pBpa variants of FtsZ,
275 which were isolated from a random library that we constructed (details to be
276 described elsewhere).
277 When probed with streptavidin-AP conjugate (against the Avi tag), the blotting
278 results show that, similar to FtsZ-K140pBpa (**Fig. 1A**, lane 4), none of these pBpa
279 variants formed photo-crosslinked FtsZ dimers (results for 11 of them are displayed in
280 **Fig. S2A**) in late stationary phase cells. When the same samples were probed with
281 antibodies against FtsZ, as shown in **Fig. 3A**, we found that the pBpa variants of the
282 FtsZ protein interact with other particular proteins apparently in a surface specific
283 fashion. Specifically, for example, when pBpa was placed at residue position 151, 166
284 or 174 (**Fig. 3A**, lanes 2, 4 and 6), all of which occupy a spatial position adjacent to
285 K140 according to the determined crystal structure of FtsZ monomer[34], a pattern of
286 photo-crosslinked products largely comparable to that of FtsZ-K140pBpa was
287 revealed (**Fig. 1A**, lane 8). Similarly, the four variants with pBpa introduced at
288 position 31, 47, 51 or 54, all of which are adjacent to each other but distant from
289 K140, also generated a pattern of photo-crosslinked products similar to each other but
290 different from that of FtsZ-K140pBpa (**Fig. 3A**, lanes 8, 10, 12 and 14). In contrast,
291 the variants with pBpa at the rest positions (**Fig. 3A**, lanes 16, 18, 20, 22, 24, 26 and
292 28), each occupying a non-adjacent spatial position, generated no or individually
293 unique patterns of crosslinked products. Collectively, these observations indicate that
294 the FtsZ proteins in the cell-pole granules of late stationary-phase cells are apparently
295 folded.
296 We next attempted to find out whether or not such cell-pole granules could
297 maintain their structure and thus be isolated as intact entities after the cells are lysed.
298 The imaging results shown in **Fig. 3B** clearly demonstrate that such granules could
299 still be clearly detected in the cell lysates. We subsequently collected the granules as
300 the centrifugation pellet of the lysed wild-type *E. coli* cells and then re-suspended it in
301 8 M urea to effectively dissolve the protein components within them, before the large
302 membrane fragments to be removed as the new pellet through another round of
303 centrifugation. Afterwards, the new supernatant was concentrated by about 10-fold
304 before the sample was resolved by SDS-PAGE. The Coomassie blue staining results,
305 displayed in **Fig. 3C**, revealed many protein bands (lane 10), with a pattern apparently
306 different from that of the total cell lysates (lane 5), suggesting that the protein
307 components present in the cell-pole granules are selected. This meanwhile
308 demonstrate that the protein composition of the cell-pole granules is clearly
309 distinguishable from that of the inclusion body, which is commonly composed of
310 several dominant proteins that are heterologously over-expressed[28].

311 We subsequently excised the protein bands that could be clearly visualized on the
312 gel for mass spectrometry analysis. As listed in **Fig. 3D**, besides FtsZ, numerous key
313 proteins that are known to function in such fundamental biological processes as
314 transcription, translation, metabolism and cell division were identified. We verified
315 the presence of five of these identified proteins, by separately expressing each as an
316 Avi-tagged form from a plasmid construct, in the pellet fraction of late
317 stationary-phase and in the supernatant fraction of log-phase cells, as shown in **Fig.**
318 **3E** (lanes 6 vs 3).
319 Our live-cell imaging analysis, performed by fusing the target protein with
320 mNeonGreen, also verified the presence of FtsA and ZapC, two proteins that we
321 identified in the cell-pole granules and are known to function in cell division[27,35], in
322 Z-ring structure of log-phase cells but in cell-pole granules of late stationary-phase
323 cells (**Fig. S2B**). By contrast, FtsL and ZapA, two proteins that we did not identify in
324 the cell-pole granules but are also known[36] and confirmed by us to be present in the
325 Z-ring structure of log-phase cells, were found to be evenly distributed in the
326 cytoplasm, rather than in the cell-pole granules, in late-stationary phase cells (**Fig.**
327 **S2B**). In addition, we demonstrated that FtsA (fused with the red fluorescent protein
328 mCherry) co-localizes with FtsZ (fused with mNeonGreen), not only in the Z-ring
329 structure of log-phase cells but also in the cell-pole granules either in late
330 stationary-phase cells or in their lysates, as shown in **Fig. S2C**. Taken together, these
331 observations suggest that the cell-pole granules apparently sequester selected proteins
332 which are important for cell growth and division. In view that the cell-pole granules
333 are only formed in the non-growing/non-dividing late-stationary phase bacterial cells,
334 we hereafter designate them as "quiescent bodies" and continue to explore their
335 biological significance by utilizing FtsZ-mNeonGreen as the biomarker.

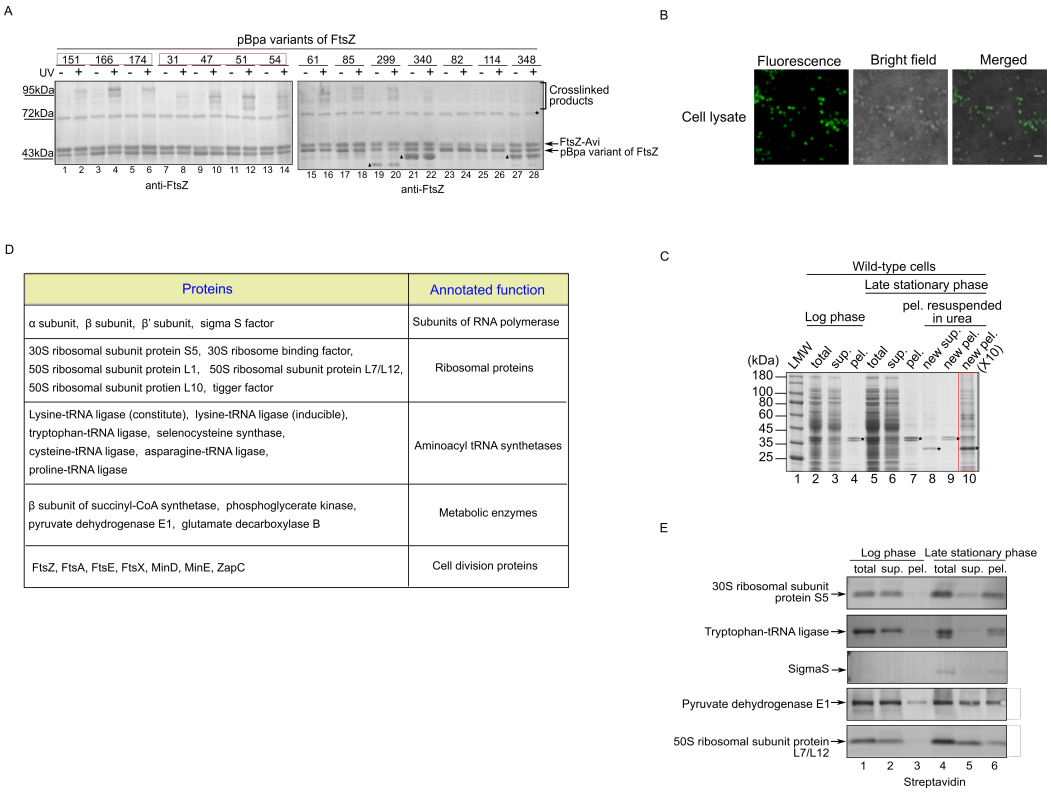

D

Proteins	Annotated function
α subunit, β subunit, β' subunit, sigma S factor	Subunits of RNA polymerase
30S ribosomal subunit protein S5, 30S ribosome binding factor, 50S ribosomal subunit protein L1, 50S ribosomal subunit protein L7/L12, 50S ribosomal subunit protien L10, tigger factor	Ribosomal proteins
Lysine-tRNA ligase (constitute), lysine-tRNA ligase (inducible), tryptophan-tRNA ligase, selenocysteine synthase, cysteine-tRNA ligase, asparagine-tRNA ligase, proline-tRNA ligase	Aminoacyl tRNA synthetases
β subunit of succinyl-CoA synthetase, phosphoglycerate kinase, pyruvate dehydrogenase E1, glutamate decarboxylase B	Metabolic enzymes
FtsZ, FtsA, FtsE, FtsX, MinD, MinE, ZapC	Cell division proteins

Figure 3. The cell-pole granules (quiescent bodies) selectively sequester proteins essential for cell growth and division.

(A) Immunoblotting results for detecting the photo-crosslinked products of the indicated pBpa variants of FtsZ in late stationary-phase *ftsZ-Avi* cells, as probed with antibodies against FtsZ. The asterisk indicates a non-specific protein band, and the triangles indicate the truncated forms of FtsZ produced due to the failure of pBpa incorporation at the replaced TAG stop codon.

(B) Fluorescence and bright field microscopic images of the cell-pole granules as detected in lysates of late stationary-phase (cultured to 24 h) cells in which the FtsZ-mNeonGreen protein was heterologously expressed in addition to the endogenous FtsZ.

(C) Coomassie blue-stained SDS-PAGE results for detecting proteins present in the total lysate (lanes 2 and 5), supernatant (lanes 3 and 6) and pellet fractions (lanes 4 and 7) of log-phase or late stationary-phase wild-type *E. coli* cells. The pellet of the lysate (as analyzed in lane 7) of late stationary-phase cells was dissolved in 8 M urea and re-centrifuged, with the new supernatant (new sup.; lane 8) being concentrated by approximately 10-fold before loaded for the gel electrophoresis (lane 10). Asterisks (in lanes 4 and 7-10) indicate the protein bands that were identified by mass spectrometry analysis as outer membrane proteins OmpA, OmpF and OmpC, which apparently ended in the pellet fraction as large outer membrane fragments that were generated during cell lysis by French Press.

(D) List of major proteins that were identified in the quiescent body-containing insoluble pellet by mass spectrometry analysis.

(E) Blotting results for analyzing the distribution of the indicated proteins, that were identified in the quiescent bodies and linked with an Avi tag, in the indicated fractions of log-phase or late stationary-phase wild-type *E. coli* cells, probed with streptavidin-AP conjugate against the Avi tag. Of note, the sigma S factor was previously reported only to be accumulated in late stationary-phase but not in log-phase bacterial cells[37].

Quiescent bodies are formed in a heterogeneous manner among individual cells.

Before our effort to identify the factors that trigger the formation of quiescent bodies, we first examined the time course of quiescent body formation during cell culturing. For this purpose, we monitored the status of the FtsZ protein by performing live-cell imaging analysis with the *ftsZ-mNeonGreen* cells cultured to particular time

points from 6 h (log-phase) to 24 h (late-stationary phase) and in the presence of rhamnose (to induce the production of the FtsZ-mNeonGreen protein).

The data displayed in **Fig. 4** reveal, remarkably, that the formation of quiescent bodies appears to be highly heterogeneous among individual cells. Specifically, at the 12 h culturing point, although the Z-ring structure became no longer visible in many cells, quiescent bodies are not yet visible in them. At the 15 h culturing point, although the Z-ring structure remained visible in some of the cells, quiescent bodies started appearing in many of the rest. At the 18 h culturing point, the Z-ring structure became no longer visible and the quiescent bodies appeared almost in all the cells. At the 21 h culturing point, quiescent bodies appear to be fully formed in all the cells. The heterogeneity of quiescent body formation is most clearly indicated by the imaging data recorded at the 15 h point, when the Z-ring structures remain visible in some of the cells while quiescent bodies are well formed in some others. Additionally, quiescent body formation seems to first start at one cell pole rather than start simultaneously at both poles in each individual cell and that each quiescent body appears to be formed in a multi-stage and progressive manner.

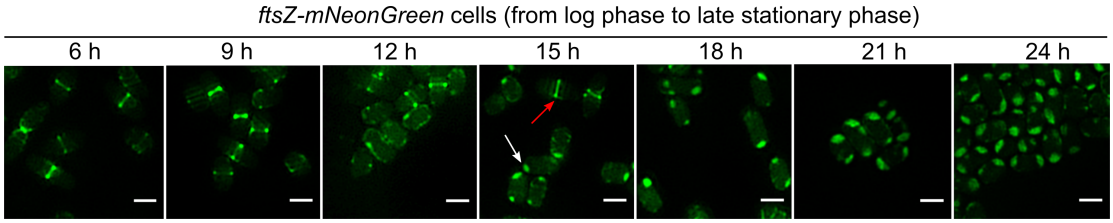

Figure 4. The formation of quiescent bodies appears to be highly heterogeneous among individual *E. coli* cells.
Fluorescence microscopic images of the *ftsZ-mNeonGreen* cells recorded at the indicated time points of culturing. Cells were grown in Luria-Bertani (LB) medium containing 0.02% rhamnose. Scale bars, 1 μm.

Formation of quiescent bodies could be effectively induced in log-phase cells that are placed in the late stationary-phase culture medium or induced by indole.

The fact that quiescent bodies start to be formed in the cells only until certain culturing points strongly suggests that their formation is triggered due to the accumulation of certain signaling molecules produced by the cells themselves during their culturing in the Luria-Bertani medium. This is somehow analogous to the effect of the quorum sensing signaling molecules that are accumulated in the culture medium when the cell density reaches a certain level[38]. We then assessed whether or not the culture medium derived from late stationary phase (of 24 h culturing) is able to induce the formation of quiescent bodies in the actively dividing log-phase cells (of 6 h culturing). Data presented in **Fig. 5A** (top panel) reveal that the Z-ring structure started to disappear after the log-phase cells were placed in the late-stationary phase culture medium for as short as 1 hour, with quiescent bodies to be fully formed almost in all the cells after approximately 4 hours. As a control, the Z-ring structure was

clearly visible in all the untreated cells after a parallel culturing for the same duration (**Fig. 5A**, bottom panel). These results indicate that certain factor, likely produced by the normal metabolic activities of the cells, was accumulated and induced the formation of quiescent bodies.

It has been documented that the catabolism of amino acids will proceed after the sugars are exhausted for bacterial cells cultured in LB medium[39]. This leads to accumulation of certain metabolic products such as ammonia and indole in the culture medium[39–41]. In light of this, we then examined whether ammonia or indole is able to substitute the late stationary-phase culture medium in inducing the formation of quiescent bodies in log-phase cells. We demonstrated that ammonia appears to be ineffective in inducing the formation of quiescent bodies in log-phase cells. By contrast, quiescent bodies became clearly visible in log-phase cells that were treated, for example, with 5 mM indole for as short as 1 hour, or 2.5 mM indole for 2 hours (**Fig. 5B**). In line with this, the FtsZ protein was significantly detected in the pellet fraction of such indole-treated log-phase cells (**Fig. 5C**, lane 6). Nevertheless, we found that quiescent bodies could still be effectively formed in late stationary-phase cells lacking the *tnaA* gene, which encodes the tryptophanase enzyme that is believed to be responsible for producing indole from L-tryptophan in bacterial cells[40,42] (**Fig. S3**). These results indicate that indole, though effective in inducing the formation of quiescent bodies in log phase cells, is still apparently not the essential factor for the formation of quiescent bodies in stationary-phase cells.

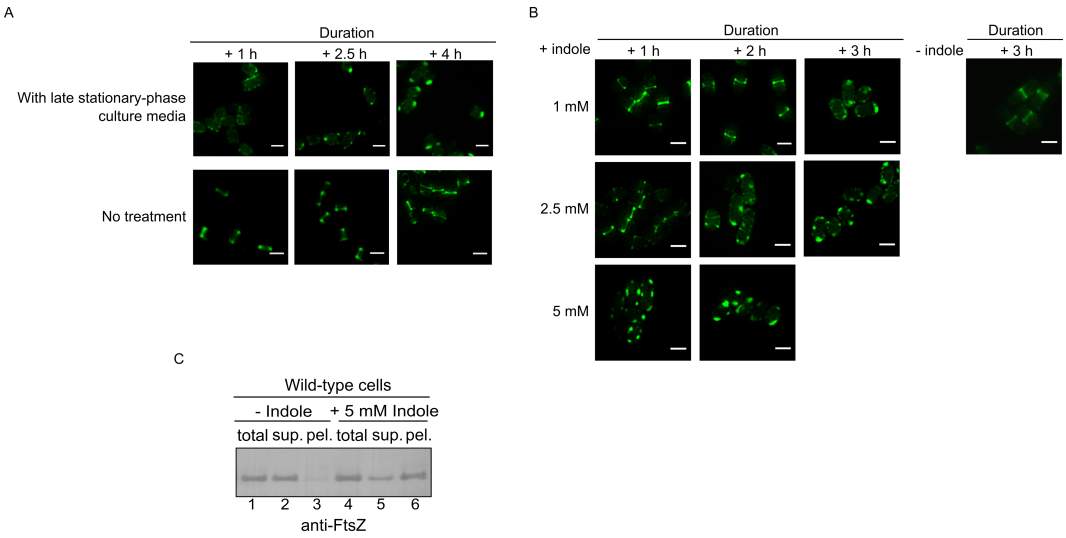

Figure 5. Late stationary-phase LB culture medium or indole is able to effectively induce the formation of quiescent bodies in log-phase *E. coli* cells.

(A) Fluorescence microscopic images of log-phase *ftsZ-mNeonGreen* cells that were placed in late stationary-phase LB culture medium for the indicated duration (top panel). The untreated log-phase cells that were further cultured were analyzed here as the negative control (bottom panel). Scale bars, 1 μm.

(B) Fluorescence microscopic images of log-phase *ftsZ-mNeonGreen* cells that were treated with indole (+ indole) of the indicated concentrations and durations. As the negative control (- indole), the cells were treated with DMSO (the solvent used for dissolving indole). Scale bars, 1 μm.

(C) Immunoblotting results for detecting the presence of FtsZ in the total cell lysate (total, lane *4*), supernatant (sup., lane 5) or pellet (pel., lane 6) fraction of the log-phase wild-type cells that were

442 treated with indole (5 mM) for 1 h, as probed with antibodies against FtsZ. Untreated cells (-
443 indole) were analyzed here as the negative control (lanes 1-3).
444
445
446 **Formation of quiescent bodies relies on the operation of cellular respiration.**
447 During the experiments described above (**Fig. 5B**), we accidentally noticed that a
448 sufficient supply of oxygen is critical for indole to exhibit its inducing effect.
449 Specifically, quiescent bodies would not be formed in the log-phase cells if the
450 induction was performed in airtight tubes and without shaking, as shown in **Fig. 6A**
451 (the - O_2 image). Given that indole was reported to be able to dissipate the proton
452 gradient across the inner membrane in *E. coli* cells [43], such an inducing effect of
453 indole might be due to its acceleration of the electron transferring process, which
454 would rely on an adequate supply of oxygen. This speculation is partly supported by
455 our observation that the inducing effect of indole on quiescent body formation would
456 be eliminated in the presence of glucose, whose metabolism was known to inhibit
457 cellular respiration[41,44], in the culture medium before the log-phase cells were treated
458 with indole even in a sufficient supply of oxygen (**Fig. 6A**; the + O_2, + Glc image).
459 We then assessed whether the occurrence of cellular respiration is essential for
460 quiescent body formation in bacterial cells. For this purpose, we examined whether or
461 not quiescent body formation will be affected either in the *ftsZ-mNeonGreen* (for the
462 imaging analysis shown in **Fig. 6B**) or in wild-type (for the immunoblotting analysis
463 shown in **Fig. 6C**) strain in which either the *nuoA* or *sdhC* gene was knocked down by
464 using the CRISPRi technology[45]. The results, as shown in **Fig. 6B** (right column
465 images), revealed that the formation of quiescent body hardly occurs in the *sdhC*
466 knockdown or rarely in the *nuoA* knockdown late-stationary phase cells. Consistently,
467 formation of quiescent bodies no longer occurs in the log-phase cells of either the
468 *sdhC* or *nuoA* knockdown strain that were treated with indole (**Fig. 6B**, middle
469 column images). In line with this failure of quiescent body formation, the
470 immunoblotting data, shown in **Fig. 6C**, indicate that little endogenous FtsZ protein
471 was detected in the pellet fraction (lanes 6 or 9) of the late stationary-phase *nuoA* or
472 *sdhC* knockdown cells. Taken together, these observations indicate that the normal
473 operation of cellular respiration is essential for the formation of quiescent bodies in
474 bacterial cells. It should be pointed out that we achieved similar results with the
475 *nouAB* or *sdhCDAB* knockout *E. coli* mutant strain.

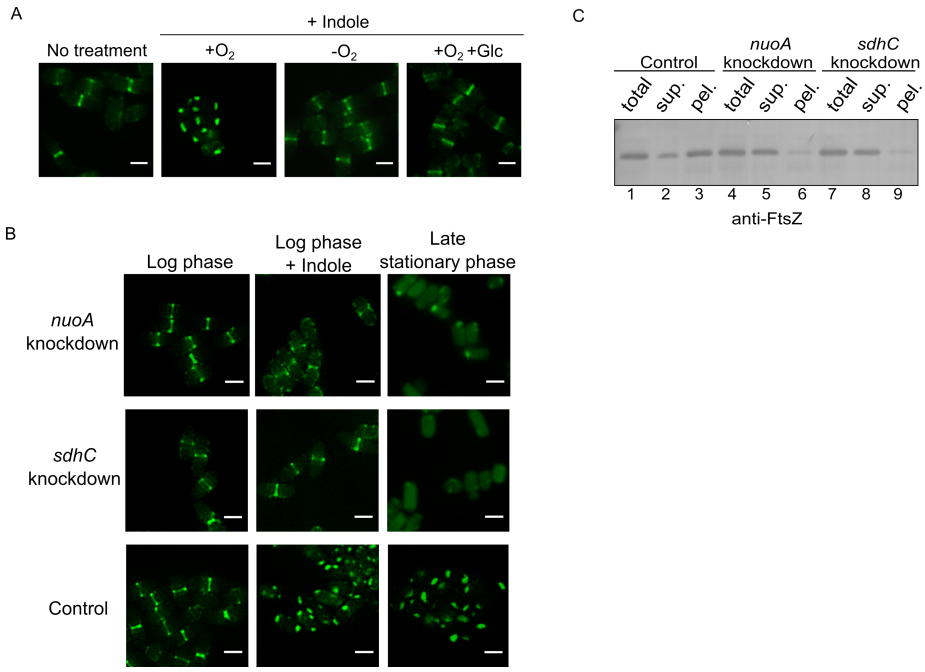

Figure 6. Normal operation of cellular respiration is essential for the formation of quiescent bodies.

(A) Fluorescence microscopic images of log-phase *ftsZ-mNeonGreen* cells that were treated with indole (5 mM) for 1 h, under the indicated conditions of oxygen and glucose supplies. Scale bars, 1 μm.

(B) Fluorescence microscopic images of log-phase (untreated or treated with indole) or late stationary-phase *ftsZ-mNeonGreen* cells possessing a knockdown of the *nuoA* or *sdhC* gene. For the control, a non-targeting crRNA (CRISPR RNA) was expressed in the *ftsZ-mNeonGreen* cells. Scale bars, 1 μm.

(C) Immunoblotting results for detecting the distribution of FtsZ in the indicated fractions of late stationary-phase *nuoA*- or *sdhC*-knockdown cells, probed with anti-FtsZ antibodies.

Quiescent bodies are dissolved in a highly heterogeneous manner among individual cells with the FtsZ protein being re-utilized to form the Z-ring structure when late stationary-phase cells are re-cultured in fresh medium.

We subsequently tried to gain insight on the biological significance of the quiescent body. To this end, we first examined the fate of the quiescent bodies when the late stationary-phase *ftsZ-mNeonGreen* cells were placed in fresh culture medium. Live-cell imaging data shown in **Fig. 7A** indicate, intriguingly, that when re-cultured in fresh LB medium lacking rhamnose (thus no new FtsZ-mNeonGreen protein would be synthesized), a time-dependent relocation of the FtsZ-mNeonGreen protein from the quiescent bodies to the Z-ring structure was clearly observed as soon as a cell starts to re-grow (marked by an increase in size; as represented by the two cells circled with white lines). By contrast, quiescent bodies remained unaltered in cells that had not yet started their re-growth (marked by a lack of size increase; as represented by the two cells circled with red lines in **Fig. 7A**).

The remarkable reversible nature of the FtsZ proteins sequestered in the quiescent bodies was further verified. Specifically, the immunoblotting results, shown in **Fig. 7B**, demonstrate that while the FtsZ protein detected in the pellet fraction of wild-type

507 (not the *ftsZ-mNeonGreen*) cells became gradually reduced (lanes 3 to 6 to 9), those
508 detected in the supernatant fraction became gradually increased (lanes 2 to 5 to 8),
509 during the re-culturing of the late stationary-phase cells. In line with this, we also
510 observed a time-dependent increase in the level of photo-crosslinked FtsZ-K140pBpa
511 homo-dimers, accompanied with a parallel decrease in the level of the
512 photo-crosslinked products between FtsZ-K140pBpa and other proteins (lanes 2-4,
513 **Fig. 7C**) in the cells that were re-cultured in fresh LB medium lacking pBpa (thus no
514 new FtsZ-K140pBpa protein would be synthesized). Taken together, these
515 observations reveal that the proteins (as represented by FtsZ) sequestered in quiescent
516 bodies could be released for functional resumption when the late stationary-phase
517 cells re-grow and re-divide in fresh medium.
518 Interestingly, the live-cell imaging data of the *ftsZ-mNeonGreen* cells, as
519 displayed in **Fig. 7A**, also clearly demonstrate that the dissolution of quiescent bodies,
520 analogous to their formation (as shown in **Fig. 4**), also occurs in a highly
521 heterogeneous manner among individual cells. It is conceivable that such a
522 heterogeneity in their formation and dissolution are related in a certain way. For
523 example, the formation of quiescent bodies in each stationary-phase cell apparently
524 occurs in multiple consecutive stages such that those more mature ones may take
525 longer time to initiate their dissolution. It follows that the time taken for the quiescent
526 bodies to initiate their dissolution in each bacterial cell may correspond to the lag time
527 during cell recovery[6,39,46].
528 We next examined whether or not the FtsZ proteins in the quiescent bodies could
529 be released when the synthesis of all proteins is suppressed by the presence of the
530 antibiotic chloramphenicol [47]. The live-cell imaging data shown in **Fig. 7D** reveal a
531 similar time-dependent disappearance of the FtsZ-mNeonGreen protein in quiescent
532 bodies in the cells that initiated their re-growth (e.g., the two white circled cells).
533 With no exception, the heterogeneity phenomenon of quiescent body dissolution was
534 once again clearly observed here (one non-growing cell whose quiescent bodies
535 remain unaltered is indicated by the red circled cell in **Fig. 7D**). Again,
536 immunoblotting results, displayed in **Fig. 7E**, clearly reveal a similar solubility
537 change of the FtsZ protein as observed above (**Fig. 7B**) during the re-culturing of the
538 wild-type (not the *ftsZ-mNeonGreen*) cells. These observations suggest that the
539 dissolution of quiescent bodies apparently does not rely on new protein synthesis and
540 thus qualifies as an early event for non-growing bacterial cells to recover.
541 Collectively, the data displayed in **Fig. 7** suggest that the proteins sequestered in
542 quiescent bodies can be effectively released to resume their functions upon cell
543 re-growth/re-division, and that the lag time during the recovery of non-growing
544 bacterial cells apparently reflect the time taken for the quiescent bodies to initiate
545 their dissolution (as further demonstrated below).

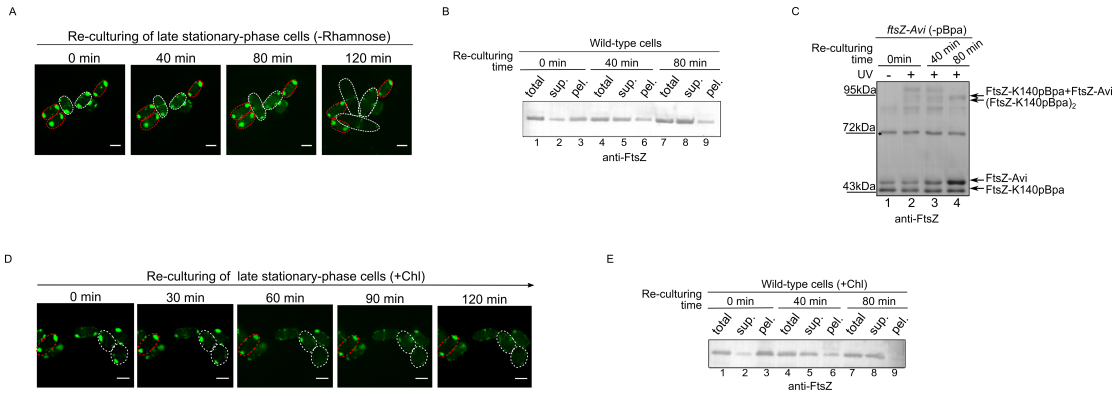

Figure 7. The quiescent bodies are dissolved in a highly heterogeneous manner among individual cells upon their re-growth/re-division releasing the sequestered FtsZ proteins that are re-utilized in forming the Z-ring structure.

(A) Live-cell fluorescence microscopic images of late stationary-phase *ftsZ-mNeonGreen* cells that were re-cultured to the indicated time points in fresh LB medium lacking rhamnose. The cells indicated by red circles did not start their re-growth while those indicated by white circles started their re-growth during the 120 min of re-culturing. (Note: one of the re-growing cells divided into two daughter cells at the 120 min re-culturing time point). Scale bars, 1 μm.

(B) Immunoblotting results for detecting the distributions of FtsZ in the supernatant (sup.) and pellet (pel.) fractions of the late stationary-phase wild-type (not the *ftsZ-mNeonGreen*) cells that were re-cultured in fresh LB medium to the indicated time points, probed with anti-FtsZ antibodies.

(C) Immunoblotting results for detecting the photo-crosslinked products of FtsZ-K140pBpa expressed in the late stationary-phase *ftsZ-Avi* cells that were re-cultured to the indicated time points in fresh LB medium lacking pBpa, probed with antibodies against FtsZ. Indicated on the right are positions of the FtsZ monomers, being FtsZ-K140pBpa and FtsZ-Avi, and the photo-crosslinked FtsZ dimers, being $(\text{FtsZ-K140pBpa})_2$ and FtsZ-K140pBpa+FtsZ-Avi.

(D) Live-cell fluorescence microscope images (recorded at 37°C) of the late stationary-phase *ftsZ-mNeonGreen* cells that were inoculated to the indicated time points in fresh LB medium containing the antibiotic chloramphenicol which inhibits the overall protein synthesis in the cells. Two cells whose quiescent bodies were dissolving are indicated by the white circles; one cell whose quiescent bodies remained unaltered during the 120 min of re-culturing is indicated by the red circle. Scale bars, 1 µm.

(E) Immunoblotting results for detecting the distributions of the FtsZ protein in the indicated fractions when the late stationary-phase wild-type (not the *ftsZ-mNeonGreen*) cells were re-cultured to the indicated time points in fresh LB medium containing chloramphenicol, probed with anti-FtsZ antibodies.

The degree of quiescent body formation in the non-growing cells is correlated with the duration of the lag time for their re-growth.

We next tried to find out whether or not the duration of lag time for the bacterial cell recovery can be correlated to the degree of quiescent body formation in the non-growing cells. For this purpose, we decided to make use of the multiple types of *E. coli* cells that form quiescent bodies to different degrees, as described above (**Figs. 4**, **5B** and **6B**). Additionally, we decided to express their lag time as the average initial doubling time upon re-division (abbreviated as re-division T_{id}), which was calculated on the basis of their re-culturing growth curves (displayed in **Fig. S5**).

The lag time measurement results of the multiple types of cells, described in **Figs. 8A-8C**, reveal a strong correlation between the duration of lag time and the degree of

587 quiescent body formation (as shown in **Figs. 4**, **5B** and **6B**) in the recovering bacterial
588 cells. First, as shown in **Fig. 8A**, the re-division T_{id} value is increased by about 3 fold
589 for cells pre-cultured for 24 h (being ~108 min) when compared with cells
590 pre-cultured for 12 h (being ~34 min). It should be pointed out that the re-division T_{id}
591 value of the cells pre-cultured for 12 h was largely comparable with that of the
592 log-phase cells (being ~26 min; equivalent to the "- indole, + O_2" bar in **Fig. 8B**).
593 Second, as shown in **Fig. 8B**, the re-division T_{id} value of the indole-treated log-phase
594 cells (the "+ indole, + O_2" bar) was about 2.5 fold (~65 min vs ~26 min) of that of the
595 non-treated cells (the "- indole, + O_2" bar). Third, as shown in **Fig. 8C**, the difference
596 in re-division T_{id} values between the late stationary phase (24 h culturing) and the
597 early stationary phase (12 h culturing) cells for either the *nuoA* or *sdhC* knockdown
598 strain was much less**,** when compared with that for the wild type control cells (in
599 which a non-targeting CRISPR RNA was transcribed). Fourth, as also shown in **Fig.**
600 **8C**, for the *sdhC* knockdown strain (in which quiescent bodies no longer form), the
601 re-division T_{id} value of its late stationary-phase cells is not higher but largely
602 comparable with that of its early stationary-phase cells.
603 Consistently, we also observed a strong correlation between the degree of
604 quiescent body formation and the level of antibiotic tolerance. For instance, as shown
605 in **Fig. 8D**, we demonstrated that the survival rate of the indole-treated log-phase *E.*
606 *coli* cells (the "+ indole, + O_2" bars), in which quiescent bodies were effectively
607 formed, was approximately 10-fold higher than that of the untreated cells (the "-
608 indole, + O_2" bars) when inoculated in fresh medium containing either ofloxacin or
609 ampicillin. Similarly, as shown in **Fig. 8E**, the survival rate of the quiescent
610 body-lacking stationary-phase *sdhC*-knockdown cells was approximately 50-fold
611 lower than that of the stationary-phase wild-type cells in which a non-targeting
612 crRNA was expressed (the "control" bars). Likewise, the survival rate of the
613 *nuoA*-knockdown cells was approximately 5-fold lower than that of the control cells
614 (**Fig. 8E**).
615 In line with the observations on lag time and antibiotic tolerance, our live-cell
616 imaging analysis with the *ftsZ-mNeonGreen* cells, as shown in **Fig. 8F**, revealed that
617 only cells (e.g., the two circled by white lines) whose quiescent bodies became
618 dissolved were eventually killed after a swelling (i.e., became invisible at a certain
619 time point after an increase in their sizes) in the presence of ampicillin during the
620 re-culturing process. By contrast, the cells (e.g., the one circled by red lines in **Fig. 8F**)
621 whose quiescent bodies maintained intact remained unaltered (i.e., remained visible in
622 their original sizes at all the time points) during such re-culturing process. These
623 results meanwhile suggest that the quiescent body probably can be viewed as a
624 biomarker to label the unawakened cells during bacterial re-culturing process.

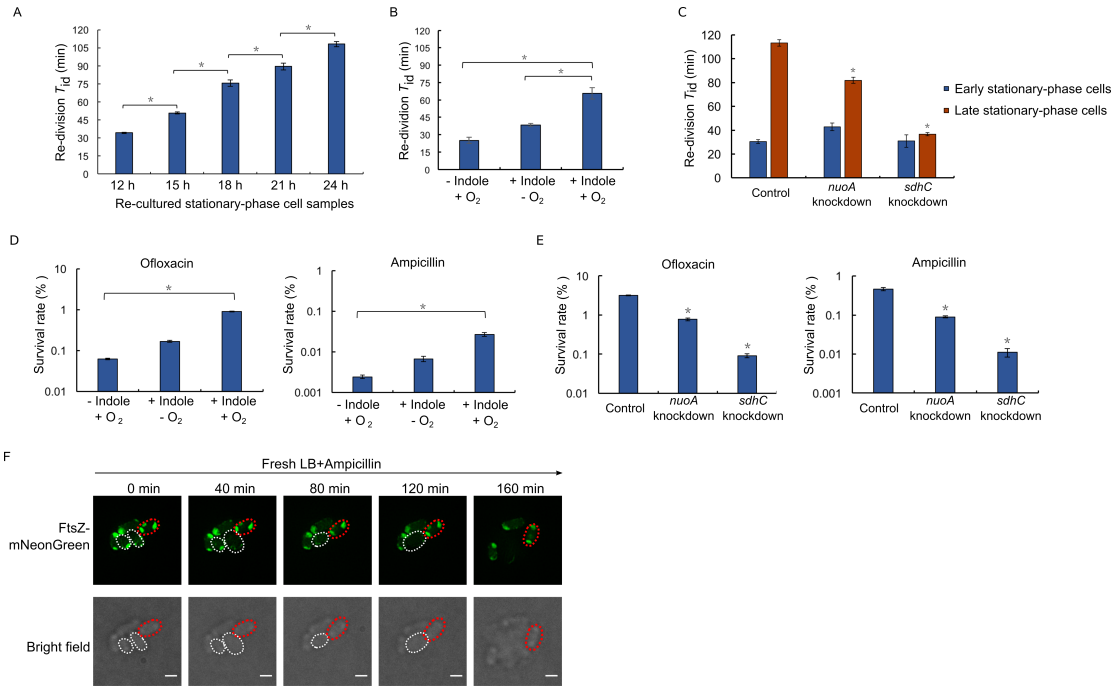

Figure 8. The degree of quiescent body formation in the non-growing bacterial cells is correlated with the duration of the lag time for their recovery.

(A) The re-division T_{id} of wild-type stationary-phase cells that were pre-cultured to the indicated time points. The cells were re-cultured (after diluting 40-fold) at 37℃ in fresh LB medium. The re-division T_{id} values were calculated based on the increase in cell number within the first 30 min of the re-culturing cells (for details, see Methods).

(B) The re-division T_{id} values of wild-type log-phase cells that were untreated (- indole) or treated (+ indole) with indole (5 mM, 1 h) and having an adequate (+ O_2) or limited (- O_2) oxygen supplies.

(C) The re-division T_{id} values of early (blue bars) or late (red bars) stationary-phase wild-type (control; in which a non-targeting crRNA was transcribed from a plasmid) and the *nuoA* or *sdhC* knockdown cells.

(D) Survival rates of wild-type log-phase cells that were untreated (- indole) or treated (+ indole) with indole, and with the adequate (+ O_2) or limited (- O_2) oxygen supply before subsequently re-cultured in fresh LB medium containing ofloxacin (5 μg/ml) or ampicillin (200 μg/ml). The survival rates were calculated as: [colony-forming units of the antibiotic-treated cells] / [colony-forming units of the antibiotic-untreated cells] ×100.

(E) Survival rates of the late stationary-phase wild-type (control), *nuoA*- or *sdhC*-knockdown cells that were re-cultured in fresh LB medium containing the indicated antibiotics. Again, a non-targeting crRNA was transcribed from a plasmid in the control cells.

The symbol ‘ * ’ in all the above panels indicates a significant difference between the compared pair of samples (P-value <0.01, t-test). At least three replicates were performed for each measurement.

(F) Live-cell fluorescence (top) or bright field (bottom) microscopic images of the late stationary-phase *ftsZ-mNeonGreen* cells that were re-cultured at 37 ℃ in fresh ampicillin-containing LB medium to the indicated time points. The re-growing cells (which were eventually lysed after a swelling, thus became invisible at a certain time point) and non-growing cells (which maintained their sizes unaltered and quiescent bodies intact all through the re-culturing process) are indicated by the white and red circles, respectively. Scale bars, 1 μm.

Discussion

Here, we accidentally discovered a new reversible subcellular structure that termed as the quiescent body in *E. coli* cells. This structure is formed only in

661 non-growing/non-dividing late stationary-phase cells and initiates to dissolve when
662 the cells re-grow/re-divide in fresh culture medium. We suppose that such a novel
663 structure is also similarly formed in other bacterial species. In retrospect, these
664 findings were made apparently as a result of our unique approach, *in vivo* protein
665 photo-crosslinking in combination with live-cell imaging, as well as our focusing on
666 the unique FtsZ protein, which assembles into the Z-ring structure.

667 Our major observations can be briefly summarized as follows. First, *in vivo*
668 protein photo-crosslinking analysis revealed that the FtsZ protein, although exists as
669 homo-oligomers in actively dividing log-phase cells, dissociates into monomers,
670 which interacts with other proteins and was detected in the pellet fraction of
671 non-dividing late stationary-phase cells (**Fig. 1**). Second, live-cell imaging analysis
672 confirmed that the FtsZ protein indeed no longer exists as the Z-ring structure, but
673 meanwhile unveiled that it exists in two cell-pole granules in each late
674 stationary-phase cell (**Fig. 2**). Third, mass spectrometry analysis revealed that such
675 cell-pole granules selectively sequester proteins (including FtsZ) that are vital for cell
676 growth and division (**Fig. 3**), and we thus named them as quiescent bodies. Fourth,
677 further live-cell imaging analysis of cells cultured to different time points showed that
678 the quiescent bodies are gradually formed in a highly heterogeneous manner among
679 individual cells (**Fig. 4**). Fifth, we demonstrated that the formation of quiescent bodies
680 can be effectively induced in log-phase cells that were placed in the late
681 stationary-phase culture medium or were treated with indole (**Fig. 5**). Sixth, gene
682 knockdown (and knockout) studies in combination with live-cell imaging analysis
683 indicated that the formation of quiescent bodies relies on the operation of cellular
684 respiration (**Fig. 6**). Seventh, live-cell imaging in combination with *in vivo* protein
685 photo-crosslinking analysis demonstrated that when the non-dividing/non-growing
686 cells were re-cultured in fresh medium, quiescent bodies can be dissolved
687 independent on protein biosynthesis, also in a heterogeneous manner among
688 individual cells, allowing the released proteins to resume their functions (**Fig. 7**).
689 Eighth, our analysis on the average re-division initial doubling time (re-division T_{id}
690 values) as well as the survival rate towards antibiotic treatments demonstrated that the
691 degree of quiescent body formation is highly correlated with the duration of lag time
692 for the non-growing bacterial cells to recover (**Fig. 8**).

693 One major implication of these findings is that the quiescent body apparently
694 functions as a biological timer for a non-growing bacterial cell to resume growth, as
695 indicated by the following observations. First, quiescent body formation among
696 individual cells appears to be highly heterogeneous such that it begins at different
697 time points in different cells and that it takes multiple stages for their maturation in
698 each cell during the culturing (**Fig. 4**). Second, the dissolution of quiescent bodies
699 also occurs in a highly heterogeneous manner among individual cells such that it
700 occurs in some cells at a very early time point while remain intact in some others even
701 at a very late time point during the re-culturing (**Fig. 7A**). Third, the duration of lag
702 time for the re-culturing is strongly correlated to the degree of quiescent body

703 formation such that the re-division T_{id} value is higher for cells that are derived from a
704 later stage of the stationary phase (**Fig. 8A**). The role of quiescent body as a
705 biological timer for bacterial cell growth resumption is apparently reflected as such
706 that the initiation of the dissolution of "younger" quiescent bodies occurs more
707 efficiently and thus takes less time, while that of the "older" ones occurs less
708 efficiently and thus takes longer time. In other words, the differential formation and
709 dissolution of quiescent bodies in individual cells may follow a "last-in-first-out (or
710 first-in–last-out)" rule[48]. The heterogeneous forming and dissolving processes of
711 quiescent bodies are schematically illustrated in **Fig. 9**.

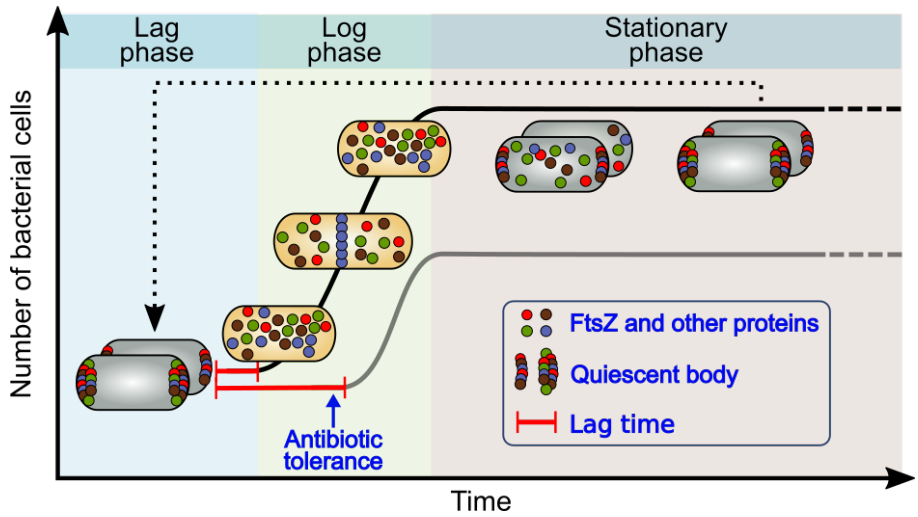

712

713 **Figure 9. The quiescent body, that is formed in the non-growing stationary phase bacterial**
714 **cells and is dissolved in the recovering cells, functions as a biological timer for non-growing**
715 **bacterial cells to resume growth.**
716

717 It has long been recognized that when bacteria are cultured in the laboratory, there
718 always exists a lag phase, in which cell growth is hardly appreciable before the cells
719 resume their growth from the non-growing state[6]. The status of the cells in this lag
720 phase remains poorly understood mainly due to their lack of metabolic activities. Our
721 discoveries reported here for the first time unveiled the occurrence of such a key
722 cellular event as the initiation of the dissolution of quiescent bodies in this unique
723 recovering stage of the bacterial cells. Their dissolution apparently does not rely on
724 new protein synthesis, thus qualifies as an early event for non-growing bacterial cells
725 to recover. By the same token, given that multiple proteins essential for cell growth
726 and division are largely sequestered in the quiescent bodies, their formation probably
727 locks the cells in a non-growing state. It follows that the dissolution of quiescent
728 bodies and the release of these key proteins represent a major barrier that the cells
729 have to overcome during the lag phase before they can initiate their re-growing
730 process.

731 The heterogeneous nature of quiescent body formation and dissolution among
732 individual cells, that would in turn generate a heterogeneity in the duration of lag time
733 taken by individual cells before their recovery, might provide a bet-hedging strategy

734 for the survival of the bacterial species[12,49,50]. Specifically, due to such heterogeneities,
735 under any particular environmental condition, only a certain portion of the
736 non-growing cells would initiate the dissolution of their quiescent bodies and thus
737 resume their growth. Such recovered cells, though may generate more offspring if the
738 condition is optimal, would become vulnerable and might be killed if the condition
739 suddenly becomes adverse again. By contrast, those cells that maintain their quiescent
740 bodies and thus remain non-growing, although not to contribute to any offspring,
741 would be highly tolerant towards the adverse conditions and thus important for
742 preventing the species from becoming extinct.
743 It has been long recognized that the dormant (persister) cells exist in an extremely
744 low number and possess an appearance hardly distinguishable from the non-dormant
745 (non-persister) ones in the bacterial cell population[2,51]. These obstacles have
746 prevented an effective investigation on them before we can find a feasible way to
747 eradicate them. In view of our findings reported here, we suppose that the formation
748 of quiescent bodies is a far more reliable distinguishable feature for defining dormant
749 (persister) bacterial cells, in comparison with the commonly described
750 non-growing/non-dividing feature[2,3]. We observed in this study that the wild-type
751 cells cultured to 12 h or the *sdhC*-knockdown cells cultured to 24 h, both of which do
752 not possess quiescent bodies although in a non-growing/non-dividing state, are able to
753 re-grow and re-divide immediately without displaying a lag time, when placed in
754 fresh LB medium (**Figs. 8A** and **8C**, respectively). This implicate that the
755 non-growing/non-dividing feature is not a reliable one for defining dormant (persister)
756 bacterial cells. Additionally, it has been commonly believed that many bacterial
757 species collected from the natural environment exist in a "viable but non-culturable"
758 state [52,53]. It is certainly worth future investigation to find out whether the presence of
759 quiescent bodies is also a common and distinguishing feature of such
760 non-growing/non-dividing bacterial cells.
761 Much needs to be further clarified on the biology of quiescent bodies. For
762 example, first, what is the chemical composition of the quiescent body and what other
763 molecules are present in addition to the proteins we identified? Second, how the
764 chemical components in the quiescent bodies are organized? Third, what is (are) the
765 key signal molecule (s) that directly trigger their formation in the stationary-phase
766 cells and how such signals are sensed by the cells to initiate the molecular events
767 leading to their formation? Fourth, why is the operation of cellular respiration
768 essential for their formation? Fifth, how are the proteins sequestered in them
769 specifically selected? Sixth, what signals trigger the initiation of their dissolution
770 when the cells are exposed to growth-permissive conditions and what are the
771 molecular events leading to their dissolution? Last but not least, we need to find out
772 whether a similar structure is present in eukaryotic cells.
773
774
775 **METHODS**

776 **Bacterial strains, plasmids and genome modifications.** Phenotypes of the bacterial
777 strains, all derived from the *E. coli* BW25113 strain, are listed in **Table S1**. The
778 plasmids used in this study are all listed in **Table S2**. All the genomic modifications
779 (to generate the *ftsZ-mNeonGreen*, *ftsZ-Avi*, Δ*nuoAB*, or Δ*sdhCDAB* strain) were
801 –red genomic recombination system[54]. All the newly generated plasmids and
802 genomic modifications were confirmed by DNA sequencing.

803 **Bacterial cell culturing.** Luria Bertani (LB) liquid (10 g/l tryptone, 5 g/l yeast extract
804 and 5 g/l NaCl) or agar-containing solid culture medium was sterilized by autoclaving.
883 g/ml ampicillin was added to the culture medium. Log-phase and late
884 stationary-phase cells refer to those that were cultured at 37℃ in test tubes shaking at
885 260 r.p.m for 6 h and 24 h, respectively, after the overnight-cultured cells were
886 diluted 100-fold dilution in LB fresh medium.

887 ***In vivo* protein photo-crosslinking of the pBpa variants of FtsZ.** This is performed
888 by using a *ftsZ* conditional knockout strain, named as LY928-Δ*ftsZ* (pJSB100), which
889 we constructed based on the LY928 strain whose genome contains the genes encoding
890 the orthogonal amino acyl-tRNA and tRNA, both needed for incorporating unnatural
891 amino acid pBpa [22], as we described earlier (22). In the LY928-Δ*ftsZ* (pJSB100) strain,
892 the wild-type FtsZ protein is expressed from the pJSB100 plasmid upon arabinose
893 induction [55]. For analyzing complementation capacity of a certain pBpa variant of
894 FtsZ, another plasmid that constitutively expressing it was transformed into the
895 LY928-Δ*ftsZ* (pJSB100) strain. Such transformed cells were then cultured in parallel
1008 g/ml ampicillin and 0.05% arabinose) and in the so-called glucose repression medium
1117 M pBpa). A variant was considered to be complement the wild-type FtsZ if the
1118 transformed cells were able to grow not only in the induction medium but also in the
1119 repression medium (to be non-complement if only to grow in the former, not in the
1120 latter). For performing the photo-crosslinking analysis, each pBpa variant of FtsZ was
1121 expressed in the self-constructed LY928-*ftsZ*-Avi strain (in which an Avi Tag was
1122 fused to the C-terminus of the endogenous wild type FtsZ protein), and the cells were
1211 M pBpa. The cells were then irradiated with UV light (365 nm) for 10 min at room
1212 temperature by using a Hoefer UVC 500 Crosslinker (Amersham Biosciences) and
1213 collected by centrifugation at 13,000 × *g* before subjecting to blotting analysis.

1214 **Fluorescence microscopic imaging.** Cell or cell lysate samples were dropped onto a
1215 glass dish (NEST biotechnology, USA) and covered with agar before micrographs
1216 were acquired at 37°C (for the re-culturing cell samples) or at 30°C (for all other
1217 samples) with an N-SIM imaging system (Nikon) by using the 2D-SIM mode, with a
1218 100×/1.49 NA oil-immersion objective (Nikon) and being excited by a 488 nm or 561
1219 nm laser beam. The 3D images were acquired with an N-SIM and a Deltavision OMX
1220 SR (GE Healthcare) imaging system by using the 3D mode. The samples were
1221 sectioned at the Z-axis every 120 nm or 240 nm. The images were further
1222 reconstructed by using the NIS-Elements AR 4.20.00 (Nikon) and the Imaris software

before further processed with the GNU image manipulation program. The oblate is calculated using the Imaris software. At least 4 images were taken and more than 50 bacterial cells were examined for each experiment. All experiments were independently repeated for at least 3 times.

Cellular fraction separation. The late stationary-phase *E. coli* cells were prepared by growing the cells at 37℃ (shaking at 260 r.p.m.) for 24 h after the overnight-cultured cells were diluted 100-fold into fresh LB medium. The cell samples in re-culturing experiments (as shown in **Fig. 7B**, **7E**) were prepared by transferring the 2-fold diluted late stationary-phase cells into fresh LB medium in the absence or presence of g/ml) and further cultured at 37℃ (shaking at 260 r.p.m.) to a particular indicated time point. The cells were then collected by centrifugation (8000 × *g*) and disrupted by a French press at 1000 MPa before centrifuged at 13,000 × *g* to separate the supernatant and pellet.

Blotting analysis. The samples including cell lysate, supernatant fraction, pellet fraction and the cells irradiated to UV were each added into the sample buffer, boiled and analyzed by tricine SDS-PAGE, or further probed with the indicated antibodies or streptavidin-AP conjugate for blotting analysis. The visualized protein bands on gels were scanned and processed using the GNU image manipulation program.

CRISPRi experiments. These were performed according to previously reported methods [45]. Briefly, plasmids carrying the crRNA that targets the *nuoA* or *sdhC* gene were transformed into the *E. coli* cells in which the proteins for recognizing and binding specific DNA sequences are expressed from the Cascade operon and the gene (*cas3* gene) encoding the protein that cleaves the target sequence was deleted. The designed DNA sequences for knocking down the *nuoA* and the *sdhC* genes were ATAGCGAATGCCCAGTGATGAGCGATGACTTC and AATGTGAAAAAACAAAGACCTGTTAATCTGGA, respectively. The control plasmid carried a non-targeting crRNA sequence CTGCTGGAGCTGGCTG CAAGGCAAGCCGCCCA. The crRNAs on the plasmids are transcribed constitutively, rather being induced.

Cell re-growth and calculation of the average initial doubling time upon re-division (re-division T_{id}). Log-phase or late stationary-phase cells of a particular type were diluted 40-fold into fresh LB medium and cultured at 37℃ with shaking (260 r.p.m.). Growth curves were prepared by measuring the OD_{600} value of the cultured cells at 30 min intervals. The re-division T_{id} value was calculated as 30 / $log_2^{Nt1/Nt0}$ min, where N_{t0} and N_{t1} are the number of cells at 0 min and 30 min, respectively. The N_{t1}/N_{t0} ratio for each batch of cultured cells was calculated based on the increase in optical density at 600 nm (the correlation between the cell number and the OD_{600} value was determined by preparing a standard curve).

Assay for cell survival after antibiotic treatment. Late stationary-phase cells or indole-induced log-phase cells were diluted 40-fold into fresh LB medium containing g/ml ampicillin and incubated at 37℃ with shaking (260 r.p.m.) for 2 h. The cells were then collected by centrifugation (to remove the culture medium and the antibiotics), re-suspended in phosphate-buffered saline (PBS) and serially diluted in PBS before being spotted on LB agar plates for Colony Formation Unit (CFU) counting. The cell survival rate was calculated as: [number of colonies formed after antibiotics treatment] / [number of colonies formed without antibiotic treatment] ×100.

Acknowledgments

We thank Harold P. Erickson (Duke University, USA) for kindly providing us the plasmid pJSB100 and Peter G. Schultz (The Scripps Research Institute, USA) for providing us the plasmids carrying genes encoding the orthogonal tRNA and amino acyl-tRNA for incorporating pBpa into target proteins. We thank Keio Collections for providing us the wild-type *E. coli* strain. We thank the Core Facilities at the School of Life Sciences, Peking University, for assistance in using the structured illumination microscopy (SIM), and we are grateful to Drs. Chunyan Shan and Xiaochen Li for their kind help in performing the fluorescence microscopic imaging analysis. We thank Dr. Wen Zhou at the Mass Spectrometry Facility of the National Center for Protein Sciences at Peking University for assistance in performing the mass spectrometry analysis. We thank Prof. Xinmiao Fu from Fujian Normal University for useful discussions. This work was supported by funds from the National Natural Science Foundation of China (No. 31670775 and 31470766 to ZYC), the National Basic Research Program of China (No. 2012CB917300 to ZYC) and Qidong-SLS Innovation Fund.

Author Contributions

Jiayu Yu and Yang Liu designed and performed the experiments, analyzed the data and drafted the manuscript. Prof. Zengyi Chang supervised this study and edited the manuscript.

Conflict of Interest

We declare that we have no conflicts of interest related to this work.

References

1352 1. Bigger, J. TREATMENT OF STAPHYLOCOCCAL INFECTIONS WITH
1353 PENICILLIN BY INTERMITTENT STERILISATION. *The Lancet* **244,** 497–500
1354 (1944).
1355 2. Burke, V., Sprague, A. & Barnes, L. V. Dormancy In Bacteria. *J. Infect. Dis.* **36,**
1356 555–560 (1925).
1357 3. Lewis, K. Persister cells, dormancy and infectious disease. *Nat. Rev. Microbiol.* **5,**
1358 48–56 (2007).
1359 4. Levin-Reisman, I. *et al.* Automated imaging with ScanLag reveals previously
1360 undetectable bacterial growth phenotypes. *Nat. Methods* **7,** 737–739 (2010).
1361 5. Monod, J. The Growth of Bacterial Cultures. *Annu. Rev. Microbiol.* **3,** 371–394
1362 (1949).
1363 6. Penfold, W. J. On the Nature of Bacterial Lag. *J. Hyg. (Lond.)* **14,** 215–241 (1914).
1364 7. Hathaway, L. J. *et al.* Capsule type of Streptococcus pneumoniae determines
1365 growth phenotype. *PLoS Pathog.* **8,** e1002574 (2012).
1366 8. Frimodt-Møller, N., Sebbesen, O. & Frølund Thomsen, V. The pneumococcus and
1367 the mouse protection test: importance of the lag phase in vivo. *Chemotherapy* **29,**
1368 128–134 (1983).
1369 9. Bättig, P., Hathaway, L. J., Hofer, S. & Mühlemann, K. Serotype-specific
1370 invasiveness and colonization prevalence in Streptococcus pneumoniae correlate with
1371 the lag phase during in vitro growth. *Microbes Infect.* **8,** 2612–2617 (2006).
1372 10. Brauner, A., Fridman, O., Gefen, O. & Balaban, N. Q. Distinguishing between
1373 resistance, tolerance and persistence to antibiotic treatment. *Nat. Rev. Microbiol.* **14,**
1374 320–330 (2016).
1375 11. Levin-Reisman, I. *et al.* Antibiotic tolerance facilitates the evolution of resistance.
1376 *Science* eaaj2191 (2017). doi:10.1126/science.aaj2191
1377 12. Fridman, O., Goldberg, A., Ronin, I., Shoresh, N. & Balaban, N. Q. Optimization
1378 of lag time underlies antibiotic tolerance in evolved bacterial populations. *Nature* **513,**
1379 418–421 (2014).
1380 13. Dai, K. & Lutkenhaus, J. ftsZ is an essential cell division gene in Escherichia coli.
1381 *J. Bacteriol.* **173,** 3500–3506 (1991).
1382 14. Erickson, H. P. Atomic structures of tubulin and FtsZ. *Trends Cell Biol.* **8,**
1383 133–137 (1998).
1384 15. Erickson, H. P., Taylor, D. W., Taylor, K. A. & Bramhill, D. Bacterial cell division
1385 protein FtsZ assembles into protofilament sheets and minirings, structural homologs of
1386 tubulin polymers. *Proc. Natl. Acad. Sci. U. S. A.* **93,** 519–523 (1996).
1387 16. Mukherjee, A. & Lutkenhaus, J. Analysis of FtsZ Assembly by Light Scattering
1388 and Determination of the Role of Divalent Metal Cations. *J. Bacteriol.* **181,** 823–832
1389 (1999).
1390 17. Erickson, H. P., Anderson, D. E. & Osawa, M. FtsZ in Bacterial Cytokinesis:
1391 Cytoskeleton and Force Generator All in One. *Microbiol. Mol. Biol. Rev.* **74,** 504–528
1392 (2010).

1393 18. Romberg, L. & Levin, P. A. Assembly Dynamics of the Bacterial Cell Division
1394 Protein FtsZ: Poised at the Edge of Stability. *Annu. Rev. Microbiol.* **57,** 125–154
1395 (2003).
1396 19. Matsui, T. *et al.* Structural reorganization of the bacterial cell-division protein FtsZ
1397 from Staphylococcus aureus. *Acta Crystallogr. D Biol. Crystallogr.* **68,** 1175–1188
1398 (2012).
1399 20. Oliva, M. A., Cordell, S. C. & Löwe, J. Structural insights into FtsZ protofilament
1400 formation. *Nat. Struct. Mol. Biol.* **11,** 1243–1250 (2004).
1401 21. Chin, J. W., Martin, A. B., King, D. S., Wang, L. & Schultz, P. G. Addition of a
1402 photocrosslinking amino acid to the genetic code of Escherichiacoli. *Proc. Natl. Acad.*
1403 *Sci. U. S. A.* **99,** 11020–11024 (2002).
1404 22. Ryu, Y. & Schultz, P. G. Efficient incorporation of unnatural amino acids into
1405 proteins in Escherichia coli. *Nat. Methods* **3,** 263–265 (2006).
1406 23. Fu, X., Shi, X., Yan, L., Zhang, H. & Chang, Z. In Vivo Substrate Diversity and
1407 Preference of Small Heat Shock Protein IbpB as Revealed by Using a Genetically
1408 Incorporated Photo-cross-linker. *J. Biol. Chem.* **288,** 31646–31654 (2013).
1409 24. Wang, Y. *et al.* A Supercomplex Spanning the Inner and Outer Membranes
1410 Mediates the Biogenesis of β-Barrel Outer Membrane Proteins in Bacteria. *J. Biol.*
1411 *Chem.* **291,** 16720–16729 (2016).
1412 25. Zhang, M. *et al.* A genetically incorporated crosslinker reveals chaperone
1413 cooperation in acid resistance. *Nat. Chem. Biol.* **7,** 671–677 (2011).
1414 26. Li, Y. *et al.* FtsZ protofilaments use a hinge-opening mechanism for constrictive
1415 force generation. *Science* **341,** 392–395 (2013).
1416 27. Ma, X., Ehrhardt, D. W. & Margolin, W. Colocalization of cell division proteins
1417 FtsZ and FtsA to cytoskeletal structures in living Escherichia coli cells by using green
1418 fluorescent protein. *Proc. Natl. Acad. Sci. U. S. A.* **93,** 12998–13003 (1996).
1419 28. Rinas, U. *et al.* Bacterial Inclusion Bodies: Discovering Their Better Half. *Trends*
1420 *Biochem. Sci.* (2017). doi:10.1016/j.tibs.2017.01.005
1421 29. Verhoeven, G. S., Dogterom, M. & den Blaauwen, T. Absence of long-range
1422 diffusion of OmpA in E. coli is not caused by its peptidoglycan binding domain. *BMC*
1423 *Microbiol.* **13,** 66 (2013).
1424 30. Harvey, B. R. *et al.* Anchored periplasmic expression, a versatile technology for
1425 the isolation of high-affinity antibodies from Escherichia coli-expressed libraries. *Proc.*
1426 *Natl. Acad. Sci. U. S. A.* **101,** 9193–9198 (2004).
1427 31. Kwiatkowska, J., Matuszewska, E., Kuczyńska-Wiśnik, D. & Laskowska, E.
1428 Aggregation of Escherichia coli proteins during stationary phase depends on glucose
1429 and oxygen availability. *Res. Microbiol.* **159,** 651–657 (2008).
1430 32. Mukherjee, A. & Lutkenhaus, J. Purification, assembly, and localization of FtsZ.
1431 *Methods Enzymol.* **298,** 296–305 (1998).
1432 33. Mori, H. & Ito, K. Different modes of SecY-SecA interactions revealed by
1433 site-directed in vivo photo-cross-linking. *Proc. Natl. Acad. Sci. U. S. A.* **103,**
1434 16159–16164 (2006).

1435 34. Löwe, J. & Amos, L. A. Crystal structure of the bacterial cell-division protein FtsZ.
1436 *Nature* **391,** 203–206 (1998).
1437 35. Durand-Heredia, J. M., Yu, H. H., De Carlo, S., Lesser, C. F. & Janakiraman, A.
1438 Identification and Characterization of ZapC, a Stabilizer of the FtsZ Ring in
1439 Escherichia coli. *J. Bacteriol.* **193,** 1405–1413 (2011).
1440 36. Ghigo, J. M. & Beckwith, J. Cell division in Escherichia coli: role of FtsL domains
1441 in septal localization, function, and oligomerization. *J. Bacteriol.* **182,** 116–129 (2000).
1442 37. Zhou, Y. & Gottesman, S. Regulation of Proteolysis of the Stationary-Phase Sigma
1443 Factor RpoS. *J. Bacteriol.* **180,** 1154–1158 (1998).
1444 38. Waters, C. M. & Bassler, B. L. Quorum sensing: cell-to-cell communication in
1445 bacteria. *Annu. Rev. Cell Dev. Biol.* **21,** 319–346 (2005).
1446 39. Sezonov, G., Joseleau-Petit, D. & D'Ari, R. Escherichia coli Physiology in
1447 Luria-Bertani Broth. *J. Bacteriol.* **189,** 8746–8749 (2007).
1448 40. Gaimster, H. & Summers, D. Regulation of Indole Signalling during the Transition
1449 of E. coli from Exponential to Stationary Phase. *PLOS ONE* **10,** e0136691 (2015).
1450 41. Wolfe, A. J. The Acetate Switch. *Microbiol. Mol. Biol. Rev.* **69,** 12–50 (2005).
1451 42. Hopkins, F. G. & Cole, S. W. A contribution to the chemistry of proteids. *J.*
1452 *Physiol.* **29,** 451–466 (1903).
1453 43. Chimerel, C., Murray, A. J., Oldewurtel, E. R., Summers, D. K. & Keyser, U. F.
1454 The Effect of Bacterial Signal Indole on the Electrical Properties of Lipid Membranes.
1455 *ChemPhysChem* **14,** 417–423 (2013).
1456 44. Basan, M. *et al.* Overflow metabolism in Escherichia coli results from efficient
1457 proteome allocation. *Nature* **528,** 99–104 (2015).
1458 45. Luo, M. L., Mullis, A. S., Leenay, R. T. & Beisel, C. L. Repurposing endogenous
1459 type I CRISPR-Cas systems for programmable gene repression. *Nucleic Acids Res.* **43,**
1460 674–681 (2015).
1461 46. Novick, A. Growth of Bacteria. *Annu. Rev. Microbiol.* **9,** 97–110 (1955).
1462 47. Wolfe, A. D. & Hahn, F. E. Mode of action of chloramphenicol IX. Effects of
1463 chloramphenicol upon a ribosomal amino acid polymerization system and its binding
1464 to bacterial ribosome. *Biochim. Biophys. Acta BBA - Nucleic Acids Protein Synth.* **95,**
1465 146–155 (1965).
1466 48. Jõers, A. & Tenson, T. Growth resumption from stationary phase reveals memory
1467 in *Escherichia coli* cultures. *Sci. Rep.* **6,** srep24055 (2016).
1468 49. Balaban, N. Q. Persistence: mechanisms for triggering and enhancing phenotypic
1469 variability. *Curr. Opin. Genet. Dev.* **21,** 768–775 (2011).
1470 50. Beaumont, H. J. E., Gallie, J., Kost, C., Ferguson, G. C. & Rainey, P. B.
1471 Experimental evolution of bet hedging. *Nature* **462,** 90–93 (2009).
1472 51. Lewis, K. Persister Cells. *Annu. Rev. Microbiol.* **64,** 357–372 (2010).
1473 52. Xu, H. S. *et al.* Survival and viability of nonculturableEscherichia coli andVibrio
1474 cholerae in the estuarine and marine environment. *Microb. Ecol.* **8,** 313–323 (1982).

1475 53. Li, L., Mendis, N., Trigui, H., Oliver, J. D. & Faucher, S. P. The importance of the
1476 viable but non-culturable state in human bacterial pathogens. *Front. Microbiol.* **5,** 258
1477 (2014).
1478 54. Lee, D. J. *et al.* Gene doctoring: a method for recombineering in laboratory and
1479 pathogenic Escherichia coli strains. *BMC Microbiol.* **9,** 252 (2009).
1480 55. Stricker, J. & Erickson, H. P. In Vivo Characterization of Escherichia coli ftsZ
1481 Mutants: Effects on Z-Ring Structure and Function. *J. Bacteriol.* **185,** 4796–4805
1482 (2003).

1483